Phase retrieval analysis of the Hobby-Eberly Telescope primary mirror segment figure error and its implication for wavefront sensing for the new wide-field upgrade

Lee, Hanshin, Hill, Gary, Hart, Michael

Hanshin Lee, Gary J. Hill, Michael Hart, "Phase retrieval analysis of the Hobby-Eberly Telescope primary mirror segment figure error and its implication for wavefront sensing for the new wide-field upgrade," Proc. SPIE 7738, Modeling, Systems Engineering, and Project Management for Astronomy IV, 77381K (5 August 2010); doi: 10.1117/12.857129

SPIE.

Event: SPIE Astronomical Telescopes + Instrumentation, 2010, San Diego, California, United States

Phase retrieval analysis of the Hobby-Eberly Telescope* primary mirror segment figure error and its implication for wavefront sensing for the new Wide-Field Upgrade

Hanshin Lee [a,†], Gary J. Hill[a], and Michael Hart[b]
[a]McDonald Observatory, University of Texas at Austin, 1 University Station C1402, Austin, TX 78712-0259, USA;
[b]Hart Scientific Consulting International L.L.C., E. Burns St., Tucson, AZ 85711, USA

ABSTRACT

Primary mirror segment figure error is potentially deleterious to the wavefront sensing in the new Hobby-Eberly Telescope (HET) Wide-Field Upgrade (WFU). Previous measurements indicated the presence of figure errors including prominent surface astigmatism on the segments, but need a systematic analysis to quantify the amounts. We developed a Phase Retrieval procedure that estimates the surface figure map by applying the iterative transform method to a set of focus-diversed images of a point source formed by the 91 segments of the 11m HET primary mirror. In this paper, we discuss this analysis and the implication of the analysis results for wavefront sensing on the upgraded HET.

Keywords: Phase retrieval, Segment surface error, Hobby-Eberly Telescope, HETDEX

1. INTRODUCTION

In the next two years, the Hobby-Eberly Telescope (HET) will be upgraded with a 22-arcmin. diameter field of view wide field corrector (WFC), a new tracker and prime focus instrument package (PFIP), and new metrology systems to support the Hobby-Eberly Dark Energy Experiment (HETDEX) [1-2]. The new corrector has improved image quality and a 10 m pupil diameter. The periphery of the field (i.e. an annular field from 18′ to 22′ diameter, called the metrology service field) will be used for guiding and wavefront sensing to provide the necessary feedback to keep the telescope correctly aligned.

The WFC will give 30 times larger observing area than the current HET corrector. It is a four-mirror design with two concave 1 meter diameter mirrors, one concave 0.9 meter diameter mirror, and one convex 0.24 meter diameter mirror. The corrector is designed for feeding optical fibers at f/3.65 to minimize focal ratio degradation, and so the chief ray from all field angles is normal to the focal surface. This is achieved with a concave spherical focal surface centered on the exit pupil. The imaging performance is 0.5 arcsec or better over the entire 22 arcmin field of view, and vignetting is minimal. As in the current HET, the WFC will track sidereal motion with respect to the optical axis of the fixed spherical primary (M1). Thus, the WFC needs to be continuously positioned to maintain its alignment in order to deliver required image quality. This demands constant monitoring and updating of the position of its components.

The WFU will employ wavefront sensing in conjunction with other metrology systems [3] to close the control loop on all axes of the telescope. The wavefront sensor (WFS) will have low-order (i.e. the first 15 terms of Zernike polynomials) sub-aperture geometry (7x7) and will provide the low-order aberration estimates and the optical alignment state of the WFC with respect to the primary mirror [4]. These data will be used primarily to provide necessary feedback for actively control the WFC focus/tip/tilt motions and primary mirror global radius of curvature, to maintain the delivered telescope image quality within specification, and secondarily to monitor the health of the telescope optical components. This will be enabled by analyzing the stellar wavefront propagating through the telescope via wavefront sensing. For the WFS, low-order aberration terms (tip/tilt/focus/coma aberrations) due to rigid-body mis-alignment of optical components (e.g. WFC internal mirrors' misalignment or the M1 tip/tilt as a whole) can be very well sensed and

* The Hobby – Eberly Telescope is operated by McDonald Observatory on behalf of the University of Texas at Austin, the Pennsylvania State University, Stanford University, Ludwig-Maximillians-Universität München, and Georg-August-Universität, Göttingen.

† Hanshin Lee.: E-mail: lee@astro.as.utexas.edu

Modeling, Systems Engineering, and Project Management for Astronomy IV,
edited by George Z. Angeli, Philippe Dierickx, Proc. of SPIE Vol. 7738, 77381K
 · doi: 10.1117/12.857129

compensated by actively adjusting the WFC rigid-body alignment state to a certain extent. Astigmatism, trefoil, and other low-order terms can also be sensed as well and give us an indication of abnormal behavior of the telescope.

However, if the wavefront contains significant amounts of high-spatial frequency components, the low-order measurements can be corrupted in such a way that Shack-Hartmann sub-aperture spots start appearing as elongated peanut-shaped PSFs with multiple blobs, confusing the spot centroid and subsequent reconstruction processes. In the HET, the primary mirror segment errors can imprint a significant amount of such high-spatial frequency errors on the stellar wavefront. In addition to individual segment alignment errors, the mirror segment figure error can be particularly deleterious to wavefront sensing. Previous measurements indicated the presence of figure errors [5] including prominent surface astigmatism on the segments, but needed a systematic analysis to quantify the amounts. We developed a Phase Retrieval procedure that estimates the surface figure error map by applying the iterative transform method to a set of focus-diversed images of a point source formed by the 91 segments of the 11 m HET primary mirror. The scope of this analysis is to understand the overall segment surface error in a more quantitative manner, but not to obtain precise surface metrology. In this paper, we discuss this analysis and the implication of the analysis results for the wavefront sensing in the WFU.

2. PHASE RETRIEVAL ANALYSIS OF HET MIRROR SEGMENT SURFACE ERROR

2.1 Brief description of phase retrieval analysis

Phase retrieval is a method for estimating the phase of a wave field propagating through an optical system (e.g. Earth atmosphere or telescope). The method takes intensity measurements of the wave field made at different observation planes, typically in proximity to the focal plane of the system with different axial separations, and iteratively searches for a phase that produces intensity data in agreement to the observed intensity measurements, based on various input constraints (e.g. the focal length of the system, pupil obscuration geometries, and pupil plane amplitude distribution). This is a further sophisticated version of the traditional through-focus (visual) analysis.

The method only requires an imaging sensor and the capability of measuring intensity data at different axial focal positions with the sensor. This greatly simplifies the measurement setup of the method and becomes ideal in systems where having separate optical metrology is nearly impossible (like in a space telescope). Also, the method was shown to be insensitive to jitter effects that could be due to vibration or air-turbulence) [6]. In addition, the measurement can be made via the imaging sensor used for the science application, thus minimizing calibration issues that can arise when using a separate metrology system. The method has been used with success in the past for image recovery [7–9], wavefront sensing for adaptive optics [10], and for diagnosing the aberrations of the Hubble Space Telescope [11,12]. It will also be used for on-orbit alignment of the segments of the James Webb Space Telescope [13]. Its potential in optical manufacturing and surface metrology is also well recognized and a number of studies [14,15] demonstrated the advantages of using this method in those applications (e.g. high accuracy, simplicity, and low cost alternative to interferometric methods).

Here, we adopt the approach given in Ref. 16 (see Figure 1 below for a schematic). This approach requires no a priori knowledge of the pupil amplitude. It uses the measured intensity data as the constraints for the retrieval procedure and estimates the pupil amplitude and phase simultaneously. We assume that the intensity data are collected at N focus positions. At the i-th observation plane, the wave field amplitude can be obtained by taking a square root of the measured two dimensional intensity data.

$$A_i = \sqrt{I_i} \tag{1}$$

These amplitudes are the reference data for the subsequent process. We start with a guessed wave field at the pupil plane, say U. This can be propagated to the Gaussian focal plane of the system in question via a Fast Fourier Transform (FFT) to form the focal plane wave field G_f.

$$G_f = FFT\{U\} \tag{2}$$

Now, the phase retrieval starts with choosing one of the measurement planes as the *source* plane and G_f is propagated to this plane, say the i-th plane. The propagation is done by the FFT-based angular spectrum method.

$$G_{fi} = \mathbf{P}_i\left[G_f\right] \tag{3}$$

where $\mathbf{P}_i$ is the forward angular spectrum propagation operator to the i-th plane. Let this propagated plane be G_{fi}. We then substitute the measured amplitude data for the amplitude of G_{fi}, which is equivalent to imposing the amplitude constraint on the wave field. Let this constrained field be H_{fi}. Now, we propagate it to the other planes, called the *target* planes, via the angular spectrum method. Let the field propagated to the j-th plane be H_{fij}. The following metric (E) is

then computed to check the level of agreement of the estimation with the measurements.

$$E = \sum_{j \neq i}^{N} \left\{ \frac{\left| A_j - \left| H_{fij} \right| \right\|^2}{A_j^2} \right\} \tag{4}$$

The ultimate goal of the phase retrieval is to find the phase of U, say θ, that minimizes E. However, intermediately, we want to find the phase of G_{fi} at the source plane that minimizes E given the measurement data at the target planes, letting φ be the phase of G_{fi}. At the first iteration, E is most likely to be large. Thus, it is necessary to find the direction along which E can be reduced. This is given by the gradient of E with respect to point-by-point phase φ as given by,

$$\frac{\partial E}{\partial \varphi} = 2 \,\mathrm{Imag}\left[G_{f\,i}\; g^{w*} \right] \tag{4}$$

where where * means complex conjugate and g^{w*} is given by

$$g^{w*} = \left[\mathbf{P}^{-1} \left\{ \sum_{j \neq i} \left[\left| A_j \right| \frac{H_{fij}}{\left| H_{fij} \right|} - H_{fij} \right] \right\} \right]^* \tag{5}$$

where $\mathbf{P}^{-1}$ is the backward angular spectrum propagation operator. The new updated phase at the source plane is then given by

$$\varphi_{new} = \varphi_{old} - \alpha \frac{\partial E}{\partial \varphi} \tag{6}$$

Here, α is the step size for this gradient search and can be determined by any line search algorithms. We use the conjugate gradient (CG) algorithm and the Brent's line search method in performing the above gradient searching procedure [17]. This procedure (called *local CG*) iterates until E is reduced by a predefined amount. The required number of iterations is usually fewer than 3. Once this is complete, the wave field with the updated phase at the i-th plane is propagated to the next measurement plane. This plane then becomes the source plane while the others (including the previous source plane) are set to be target planes and the same procedures used for the previous i-th plane are repeated. After this procedure (called *global CG*) is complete for all measurement planes, the updated wave field at the last source plane is propagated to the focal plane and then back to the pupil plane. Pupil plane constrains, such as pupil obscuration geometries, are then applied to the updated pupil wave field. The entire procedure is repeated until E becomes below a pre-defined level.

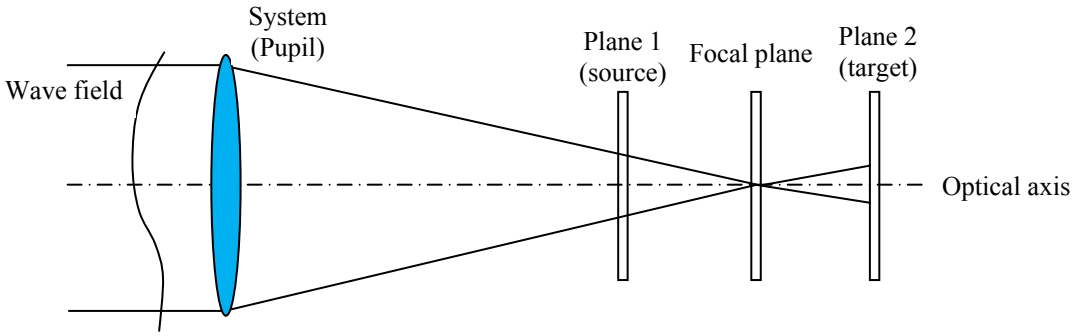

Figure 1 A schematic of the phase retrieval procedure. Here, Plane 1 is the source while Plane 2 is the target. The input wave field propagates to the focal plane and then to Plane 1. The wave field is then amplitude-constrained by using the intensity measurement in Plane 1.

Because the phase retrieval results in a wrapped phase estimate (2π modulo), it was necessary to unwrap the estimated phase. We use the Brach-cut 2D phase unwrapping algorithm [18].

2.2 Data set and analysis result

Figure 2 The HET facility (left)[5] and the CCAS tower (right)[16].

Previous reports on the HET image quality [5] indicated the presence of figure errors including prominent surface astigmatism on the segments, but need a systematic analysis to quantify the amounts. In an effort to characterize various M1 segment errors, a method based on a shearing laser interferometer has been applied. The instrument was placed at the center of curvature (CoC) of the primary mirror (26.2 m away from the M1 vertex), looking down to the M1. Although this was mainly for sensing the segment tip/tilt/piston, it was quickly realized that piston sensing was hard enough and tip/tilt sensing was less accurate than expected. In part, this is owing to the intrinsic sensitivity of single-wavelength interferometric method to various external disturbances (e.g. vibration and dome seeing). This indirectly implies that sensing surface figure error using this method would have been even harder [19].

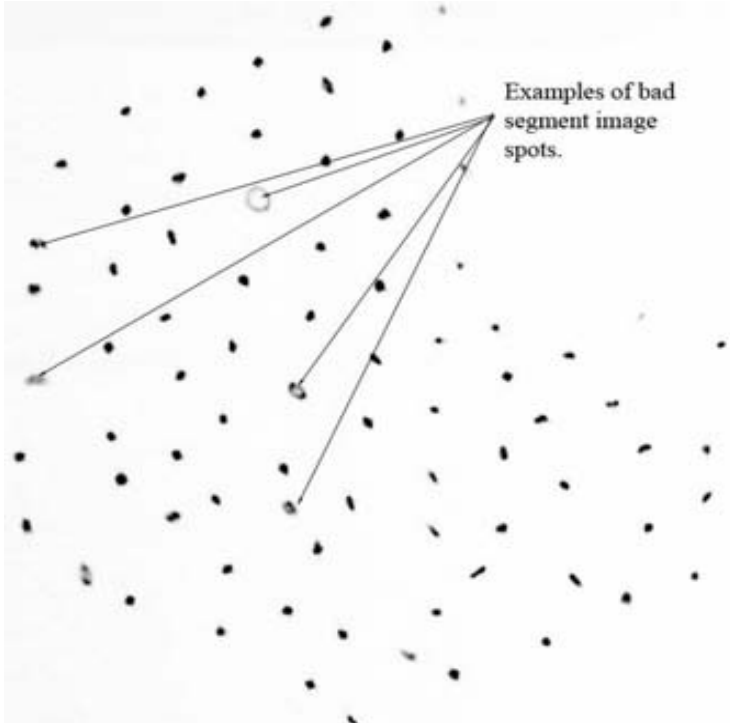

Figure 3 The bursted pinhole images formed by individual mirror segments at the best focus position of the camera. Many of the pinhole images show astigmatic ellipse, indicating the presence of surface astigmatism [5].

Subsequently, the Hartmann Extra-Focal Imager (HEFI) was designed for use at the primary mirror CoC to characterize segment alignment, figure, and radius of curvature, and the ensemble image quality of the primary mirror[5]. The instrument is housed in the Center-of-Curvature Alignment System (CCAS) tower (Figure 2). The device is mounted to the existing Mirror Alignment Recovery System (MARS) [19] optical bench and consists of a camera, ~20 μm diameter pinhole illuminated by a light source at 632.8 nm, and a retractable fold mirror. The pinhole size is chosen to be smaller than the Airy disk size (35 μm) of the PSF given by each regular hexagonal segment (1154.7 mm in apex-to-apex distance with 26163.92 mm focal length). The camera is on a linear stage with 10 μm resolution that can be moved along the folded optical axis to record the pinhole image off the primary mirror at, in front of, or behind CoC. The pinhole images formed by individual mirror segments can be "bursted" into a hexagonal array by slightly tilting the mirror segments for individual inspection. Aberrations due to this intentional segment tilt are negligible. An example picture of this bursted image is shown in Figure 3. Many of the mirror segments form astigmatic pinhole images, indicating the presence of surface astigmatism.

While the images were bursted into the hexagonal array, the camera was stepped through the focus and took several extra- and intra-focus images. Due to the tracker obstructing part of the primary mirror, the through-focus images from one set of the segments were taken first while the tracker was moved to the left edge of the x track and then the images from the other segment were measured

while the tracker was moved to the right edge of the x track. In Figure 3, images of the segments obscured by the tracker at north-east are not visible. We used the data set taken in August 25, 2008. Some of the through-focus images are shown in Figure 4. The focus range is about 10 mm between two extreme extra-focus images (890 and 1890 in encoder unit) with 10 μm stepping resolution. The image clearly shows typical astigmatic image shape in addition to double blobs that may be attributed to other higher-order surface aberrations. Most of the images are small enough to be embedded into a 128 x 128 grid for the phase retrieval. Some of the images have poor signal-to-noise ratio (like the first two top-left images). These images were not included in the analysis.

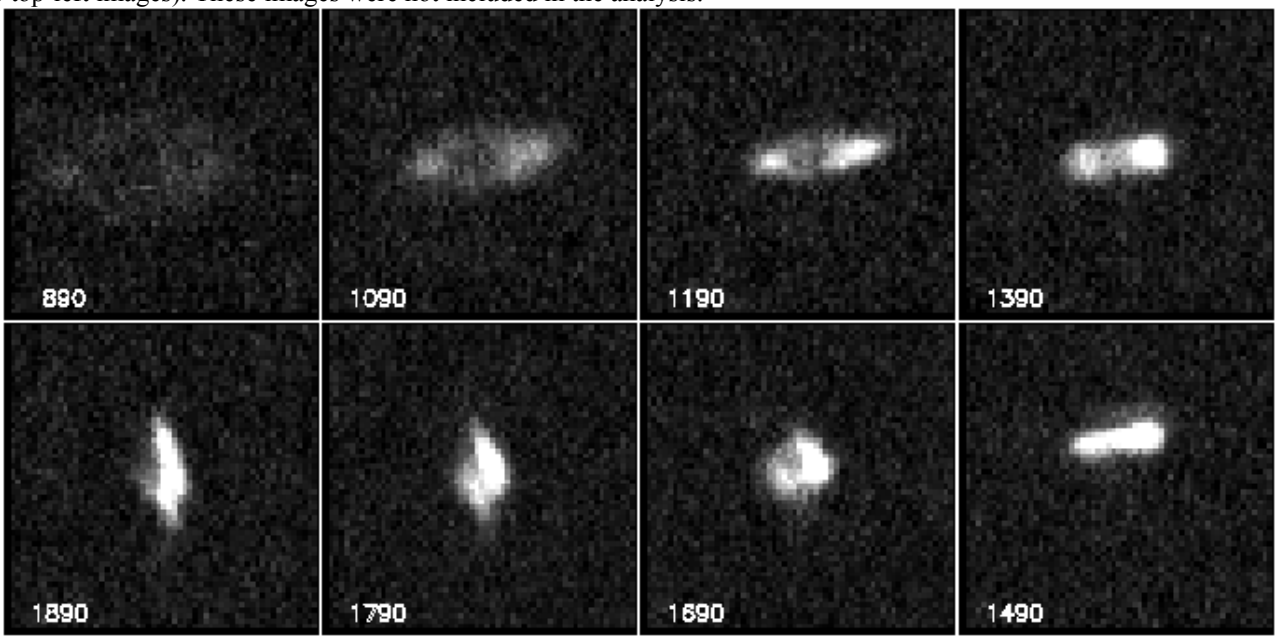

Figure 4 An example set of through-focus images by one of the 91 hexagonal mirror segments. The focus position is shown in each image in 10 μm unit. The image clearly shows typical astigmatic image shape in addition to double blobs that may be attributed to other higher-order surface aberrations.

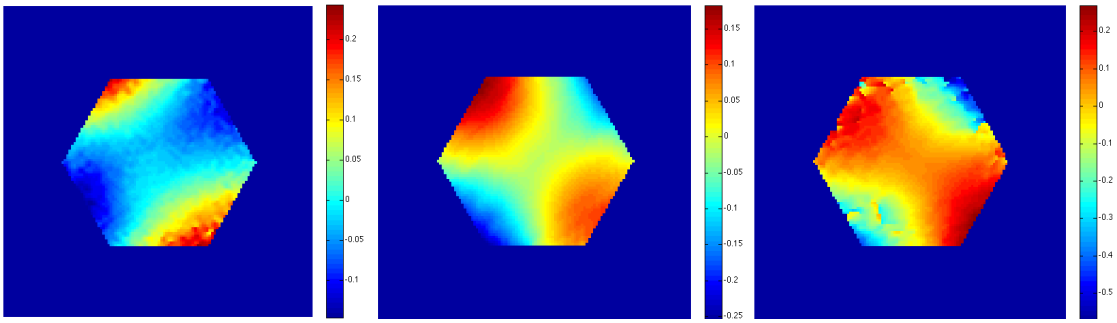

Figure 5 The surface maps of three mirror segments, estimated by the phase retrieval procedure.

There are 11 through-focus images per segment, but about half of them are background limited (those at the extreme focus positions in particular, have low SNR). On average, four through-focus images per segment were used in the phase retrieval procedure. Due to the iterative and computation-intensive nature of the phase-retrieval, the procedure arrived at an optimal estimate after 50 global CG iterations on average. Each global CG included a maximum of 3 local CG iterations, and at least 2 linear search iterations were required. In total, 1200 iterations were required to analyze one set of four through-focus images, which took about 3 min, although running the computation on a multi-core computer clearly improved the speed (less than a minute). The phase retrieval code is written in Fortran90 with Openmp [20] for code parallelization. In Figure 5, the estimated surface maps of three mirror segments are shown. The color scale is in waves at 632.8 nm. The surface maps reveal consistent astigmatic surface error (i.e. saddle shape). The estimates show small-scale structures like those in the left panel. The estimate shown on the right panel illustrates rather abrupt phase

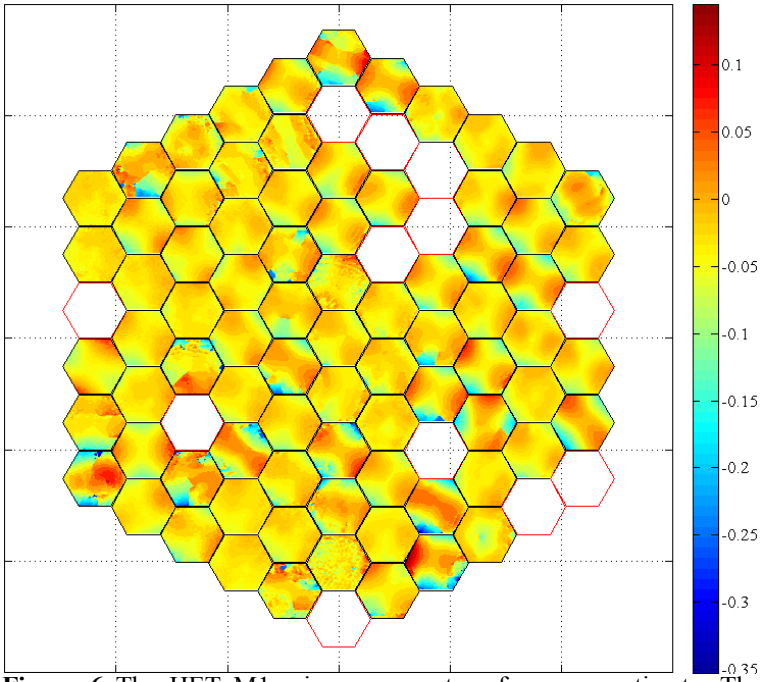

Figure 6 The HET M1 mirror segment surface map estimate. The color scale is in wave at 632.8 nm. Empty segments are due to no available through-focus image or too low signal.

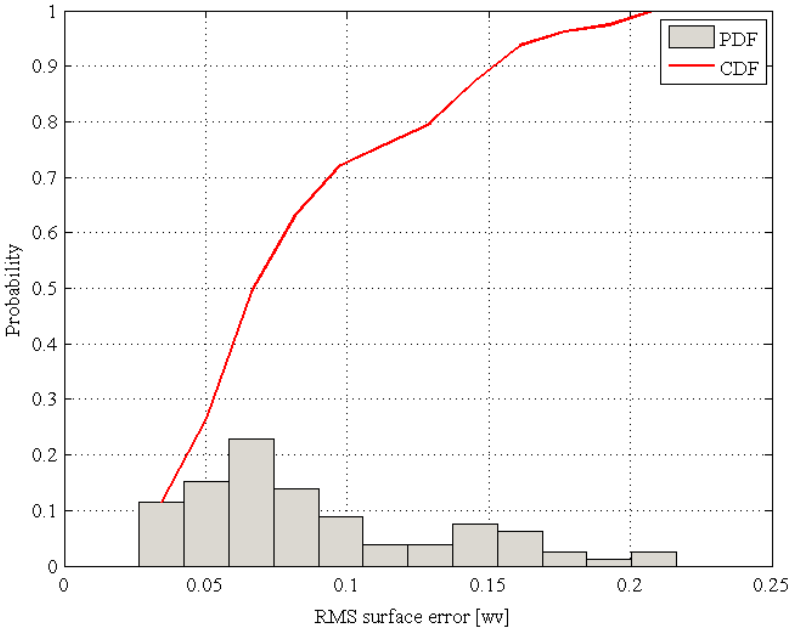

Figure 7 The distribution of the rms surface errors of the estimated segment surface maps. Both the histogram (PDF) and the cumulative distribution function (PDF) are normalized by 78 (the number of estimated segments). Note that wv is 550 nm.

change near the top right corner of the map. At the time of writing, their origin is unknown. These might be associated with, for example, abrupt variations in the mirror coating thickness or mid-spatial scale surface structures, but may well be due to variations in dome seeing.

Estimates of all mirror segment surface maps are shown in Figure 6. There are 12 empty segment slots in the figure. For these segments, either no through-focus image was available for these segments or the existing images of some of these segments were of too low quality (SNR too low). This estimate indicates that the majority of the mirror segments show some surface astigmatism. Like the ones shown in Figure 5, some of the estimates show small-scale bumpy structures and some of them show rather abrupt phase change. Segments with these features seem to gather around the left half of the M1 array. Those in the right half seem to have been less affected by these effects. The images of the left and right half of the segments were taken at different times, thus the dome seeing condition may have been different between the two measurement times, and we suspect this may be the cause.

The distribution of the rms surface error is derived from these estimated surface maps and plotted in Figure 7. The histogram (PDF) shows the distribution and the red curve shows the cumulative distribution (CDF). Both are normalized by the total number of estimated segments (78). Note that wavelength scale in this figure is 550 nm. The distribution indicates that approximately 98 % of the estimated segments have less than 0.2 wave rms surface error. Except a few, the surface error is associated with surface astigmatism. Other higher-order surface aberrations are found to be less significant.

2.3 Implication for wavefront sensing in the HET wide field upgrade

In the WFU, we plan to use low-order Shack-Hartmann wavefront sensors to monitor and control the alignment of the WFC with respect to the primary mirror. One of the effects that can degrade the WFS performance is the M1 segment surface deformation (surface astigmatism in particular). In the presence of significant segment surface error, the stellar wavefront that is sensed by the WFS can contain significant amounts of high-spatial frequency components. This can

corrupt the WFS measurement in such a way that individual SH sub-aperture spots start appearing as elongated peanut-shaped PSFs with multiple blobs. This can confuse the spot centroid and subsequent reconstruction processes, leading to incorrect aberration estimates and to a large fluctuation in WFC alignment correction along a track.
In a companion paper, we present a detailed analysis to investigate the impact of the M1 segment surface astigmatism on the WFS performance [4]. This analysis indicates that the rms segment surface astigmatism should be less than a quarter of wave at 550 nm in order for the WFS-based alignment correction to be accurate enough that the WFC alignment can be maintained to the specifications. Based on the phase retrieval analysis presented here, the expected surface astigmatism should be less than 0.2 wave at 550 nm at the 98% level. This implies that the M1 segment surface astigmatism at current levels is unlikely to affect the WFS performance significantly.

3. SUMMARY

In this paper, we presented the phase retrieval analysis of the HET primary mirror (M1) segment surface error. The phase retrieval procedure analyzes intensity data measured at multiple extra-focal positions and estimates the best pupil phase map that produces intensity patterns in agreement with the measurement data. We applied this procedure to the through-focus pinhole images from individual mirror segments, taken by the HEFI instrument at the CCAS tower of the HET. The analysis clearly revealed the astigmatic pattern in the estimated segment surface maps and allowed us to quantify the amount of the surface errors, surface astigmatism in particular. The analysis indicates that the surface astigmatism amounts to 0.2 waves at 550 nm at the 98% level. In the mean time, the WFS analysis has indicated that the M1 segment surface astigmatism should be less than 0.25 waves (@550 nm) at the 99% level in order for the wavefront sensor-based alignment correction to be accurate enough that the WFC alignment can be maintained to the specifications. This implies that the M1 segment surface astigmatism is unlikely to affect the WFS performance of the upgraded HET, significantly. Because the phase retrieval analysis was conducted for one set of HEFI data, the outcome may not be representative over a long period of time. Performing this analysis on a regular basis to monitor the segment surface error would be useful in this respect.

ACKNOWLEDGEMENTS

We thank Phillip MacQueen and the Staff of the HET for obtaining the data on which this paper is based. We thank in particular Steve Odewahn for processing the images.

REFERENCES

[1] R. Savage, et al., "Current Status of the Hobby-Eberly Telescope wide field upgrade," Proc. SPIE, 7733-149 (2010)
[2] G. J. Hill, et al., "The Hobby-Eberly Telescope Dark Energy Experiment," AIP Conference Proceedings, 773 224-223 (2004).
[3] H. Lee, et al., "Metrology systems for the active alignment control of the Hobby-Eberly Telescope wide-field upgrade," Proc. SPIE, 7739-28 (2010).
[4] H. Lee, et al., "Analysis of active alignment control of the Hobby-Eberly Telescope Wide Field Corrector using Shack-Hartmann wavefront sensors," Proc. SPIE, 7738-18 (2010).
[5] J. A. Booth, et al., "The Hobby-Eberly Telescope: Performance upgrades, status, and plans," Proc. SPIE 5489, 288-299 (2004).
[6] Andrew E. Lowman , et al., "Phase Retrieval Camera for Testing NGST Optics," Proc. SPIE 4850, 329-335 (2003).
[7] R. W. Gerchberg and W. O. Saxton, "A practical algorithm for the determination of the phase from image and diffraction plane pictures," Optik (Jena) 35, 237–246 (1972).
[8] J. R. Fienup, "Reconstruction of an object from the modulus of its Fourier transform," Optics Letters 3, 27–29 (1978).
[9] J. N. Cederquist, et al., "Phase retrieval from experimental far-field data," Optics Letters 13, 619621 (1988).
[10] J. N. Cederquist, et al., "Wave-front phase estimation from Fourier intensity measurements," J. Opt. Soc. Am. A 6, 1020–1026 (1989).
[11] J. R. Fienup, "Phase-retrieval algorithms for a complicated optical system," Appl. Opt. 32, 1737–1746 (1993).

[12] J. R. Fienup, et al., "Hubble space telescope characterized by using phase retrieval algorithms," Appl. Opt. 32, 1747–1768 (1993).
[13] B. H. Dean, et al., "Phase retrieval algorithm for JWST Flight and Testbed Telescope," Proc. SPIE 6265, 626511 (2006).
[14] G. R. Brady and J. R. Fienup, "Nonlinear optimization algorithm for retrieving the full complex pupil function," Optics Express 14, 474-486 (2006).
[15] G.R. Brady and J.R. Fienup, "Measurement of an Optical Surface using Phase Retrieval," , 2006 Topical Meeting on Optical Fabrication and Testing (Optical Society of America, Washington, DC, 2006), paper OFWA5.
[16] G.R. Brady and J.R. Fienup, "Application of Phase Retrieval to Precision Optical Metrology," in Precision Interferometric Metrology, 2005 Summer Topical Meeting of the American Society for Precision Engineering, 20-22 July 2005, Middletown, CT.
[17] W. H. Press et al., Numerical Recipes in Fortran 90, 2nd ed. (Cambridge University Press, 1996).
[18] D. C. Ghiglia and M. D. Pritt, Two-Dimensional Phase Unwrapping: Theory, Algorithms and Software (Wiley-Interscience, 1998).
[19] M. J. Wolf, et al., "Mirror Alignment Recovery System (MARS) on the Hobby-Eberly Telescope," Proc. SPIE 4837, 714-725 (2003).
[20] The OpenMP: API specification for parallel programming, http://openmp.org/wp/